Measurement of the absolute branching fraction of the singly Cabibbo suppressed decay $\Lambda_c^+ \to p\eta'$

M. Ablikim,[1] M. N. Achasov,[11,b] P. Adlarson,[70] M. Albrecht,[4] R. Aliberti,[31] A. Amoroso,[69a,69c] M. R. An,[35] Q. An,[66,53] X. H. Bai,[61] Y. Bai,[52] O. Bakina,[32] R. Baldini Ferroli,[26a] I. Balossino,[27a] Y. Ban,[42,g] V. Batozskaya,[1,40] D. Becker,[31] K. Begzsuren,[29] N. Berger,[31] M. Bertani,[26a] D. Bettoni,[27a] F. Bianchi,[69a,69c] J. Bloms,[63] A. Bortone,[69a,69c] I. Boyko,[32] R. A. Briere,[5] A. Brueggemann,[63] H. Cai,[71] X. Cai,[1,53] A. Calcaterra,[26a] G. F. Cao,[1,58] N. Cao,[1,58] S. A. Cetin,[57a] J. F. Chang,[1,53] W. L. Chang,[1,58] G. Chelkov,[32,a] C. Chen,[39] Chao Chen,[50] G. Chen,[1] H. S. Chen,[1,58] M. L. Chen,[1,53] S. J. Chen,[38] S. M. Chen,[56] T. Chen,[1] X. R. Chen,[28,58] X. T. Chen,[1] Y. B. Chen,[1,53] Z. J. Chen,[23,h] W. S. Cheng,[69c] S. K. Choi,[50] X. Chu,[39] G. Cibinetto,[27a] F. Cossio,[69c] J. J. Cui,[45] H. L. Dai,[1,53] J. P. Dai,[73] A. Dbeyssi,[17] R. E. de Boer,[4] D. Dedovich,[32] Z. Y. Deng,[1] A. Denig,[31] I. Denysenko,[32] M. Destefanis,[69a,69c] F. De Mori,[69a,69c] Y. Ding,[36] J. Dong,[1,53] L. Y. Dong,[1,58] M. Y. Dong,[1,53,58] X. Dong,[71] S. X. Du,[75] P. Egorov,[32,a] Y. L. Fan,[71] J. Fang,[1,53] S. S. Fang,[1,58] W. X. Fang,[1] Y. Fang,[1] R. Farinelli,[27a] L. Fava,[69b,69c] F. Feldbauer,[4] G. Felici,[26a] C. Q. Feng,[66,53] J. H. Feng,[54] K. Fischer,[64] M. Fritsch,[4] C. Fritzsch,[63] C. D. Fu,[1] H. Gao,[58] Y. N. Gao,[42,g] Yang Gao,[66,53] S. Garbolino,[69c] I. Garzia,[27a,27b] P. T. Ge,[71] Z. W. Ge,[38] C. Geng,[54] E. M. Gersabeck,[62] A. Gilman,[64] K. Goetzen,[12] L. Gong,[36] W. X. Gong,[1,53] W. Gradl,[31] M. Greco,[69a,69c] L. M. Gu,[38] M. H. Gu,[1,53] Y. T. Gu,[14] C. Y. Guan,[1,58] A. Q. Guo,[28,58] L. B. Guo,[37] R. P. Guo,[44] Y. P. Guo,[10,f] A. Guskov,[32,a] T. T. Han,[45] W. Y. Han,[35] X. Q. Hao,[18] F. A. Harris,[60] K. K. He,[50] K. L. He,[1,58] F. H. Heinsius,[4] C. H. Heinz,[31] Y. K. Heng,[1,53,58] C. Herold,[55] M. Himmelreich,[31,d] G. Y. Hou,[1,58] Y. R. Hou,[58] Z. L. Hou,[1] H. M. Hu,[1,58] J. F. Hu,[51,i] T. Hu,[1,53,58] Y. Hu,[1] G. S. Huang,[66,53] K. X. Huang,[54] L. Q. Huang,[28,58] X. T. Huang,[45] Y. P. Huang,[1] Z. Huang,[42,g] T. Hussain,[68] N. Hüsken,[25,31] W. Imoehl,[25] M. Irshad,[66,53] J. Jackson,[25] S. Jaeger,[4] S. Janchiv,[29] E. Jang,[50] J. H. Jeong,[50] Q. Ji,[1] Q. P. Ji,[18] X. B. Ji,[1,58] X. L. Ji,[1,53] Y. Y. Ji,[45] Z. K. Jia,[66,53] H. B. Jiang,[45] S. S. Jiang,[35] X. S. Jiang,[1,53,58] Y. Jiang,[58] J. B. Jiao,[45] Z. Jiao,[21] S. Jin,[38] Y. Jin,[61] M. Q. Jing,[1,58] T. Johansson,[70] N. Kalantar-Nayestanaki,[59] X. S. Kang,[36] R. Kappert,[59] M. Kavatsyuk,[59] B. C. Ke,[75] I. K. Keshk,[4] A. Khoukaz,[63] R. Kiuchi,[1] R. Kliemt,[12] L. Koch,[33] O. B. Kolcu,[57a] B. Kopf,[4] M. Kuemmel,[4] M. Kuessner,[4] A. Kupsc,[40,70] W. Kühn,[33] J. J. Lane,[62] J. S. Lange,[33] P. Larin,[17] A. Lavania,[24] L. Lavezzi,[69a,69c] Z. H. Lei,[66,53] H. Leithoff,[31] M. Lellmann,[31] T. Lenz,[31] C. Li,[43] C. Li,[39] C. H. Li,[35] Cheng Li,[66,53] D. M. Li,[75] F. Li,[1,53] G. Li,[1] H. Li,[66,53] H. Li,[47] H. B. Li,[1,58] H. J. Li,[18] H. N. Li,[51,i] J. Q. Li,[4] J. S. Li,[54] J. W. Li,[45] Ke Li,[1] L. J. Li,[1] L. K. Li,[1] Lei Li,[3] M. H. Li,[39] P. R. Li,[34,j,k] S. X. Li,[10] S. Y. Li,[56] T. Li,[45] W. D. Li,[1,58] W. G. Li,[1] X. H. Li,[66,53] X. L. Li,[45] Xiaoyu Li,[1,58] Y. G. Li,[42,g] Z. X. Li,[14] H. Liang,[30] H. Liang,[1,58] H. Liang,[66,53] Y. F. Liang,[49] Y. T. Liang,[28,58] G. R. Liao,[13] L. Z. Liao,[45] J. Libby,[24] A. Limphirat,[55] C. X. Lin,[54] D. X. Lin,[28,58] T. Lin,[1] B. J. Liu,[1] C. X. Liu,[1] D. Liu,[17,66] F. H. Liu,[48] Fang Liu,[1] Feng Liu,[6] G. M. Liu,[51,i] H. Liu,[34,j,k] H. B. Liu,[14] H. M. Liu,[1,58] Huanhuan Liu,[1] Huihui Liu,[19] J. B. Liu,[66,53] J. L. Liu,[67] J. Y. Liu,[1,58] K. Liu,[1] K. Y. Liu,[36] Ke Liu,[20] L. Liu,[66,53] Lu Liu,[39] M. H. Liu,[10,f] P. L. Liu,[1] Q. Liu,[58] S. B. Liu,[66,53] T. Liu,[10,f] W. K. Liu,[39] W. M. Liu,[66,53] X. Liu,[34,j,k] Y. Liu,[34,j,k] Y. B. Liu,[39] Z. A. Liu,[1,53,58] Z. Q. Liu,[45] X. C. Lou,[1,53,58] F. X. Lu,[54] H. J. Lu,[21] J. G. Lu,[1,53] X. L. Lu,[1] Y. Lu,[7] Y. P. Lu,[1,53] Z. H. Lu,[1] C. L. Luo,[37] M. X. Luo,[74] T. Luo,[10,f] X. L. Luo,[1,53] X. R. Lyu,[58] Y. F. Lyu,[39] F. C. Ma,[36] H. L. Ma,[1] L. L. Ma,[45] M. M. Ma,[1,58] Q. M. Ma,[1] R. Q. Ma,[1,58] R. T. Ma,[58] X. Y. Ma,[1,53] Y. Ma,[42,g] F. E. Maas,[17] M. Maggiora,[69a,69c] S. Maldaner,[4] S. Malde,[64] Q. A. Malik,[68] A. Mangoni,[26b] Y. J. Mao,[42,g] Z. P. Mao,[1] S. Marcello,[69a,69c] Z. X. Meng,[61] G. Mezzadri,[27a] H. Miao,[1] T. J. Min,[38] R. E. Mitchell,[25] X. H. Mo,[1,53,58] N. Yu. Muchnoi,[11,b] Y. Nefedov,[32] F. Nerling,[17,d] I. B. Nikolaev,[11,b] Z. Ning,[1,53] S. Nisar,[9,l] Y. Niu,[45] S. L. Olsen,[58] Q. Ouyang,[1,53,58] S. Pacetti,[26b,26c] X. Pan,[10,f] Y. Pan,[52] A. Pathak,[30] M. Pelizaeus,[4] H. P. Peng,[66,53] K. Peters,[12,d] J. L. Ping,[37] R. G. Ping,[1,58] S. Plura,[31] S. Pogodin,[32] V. Prasad,[66,53] F. Z. Qi,[1] H. Qi,[66,53] H. R. Qi,[56] M. Qi,[38] T. Y. Qi,[10,f] S. Qian,[1,53] W. B. Qian,[58] Z. Qian,[54] C. F. Qiao,[58] J. J. Qin,[67] L. Q. Qin,[13] X. P. Qin,[10,f] X. S. Qin,[45] Z. H. Qin,[1,53] J. F. Qiu,[1] S. Q. Qu,[56] K. H. Rashid,[68] C. F. Redmer,[31] K. J. Ren,[35] A. Rivetti,[69c] V. Rodin,[59] M. Rolo,[69c] G. Rong,[1,58] Ch. Rosner,[17] S. N. Ruan,[39] H. S. Sang,[66] A. Sarantsev,[32,c] Y. Schelhaas,[31] C. Schnier,[4] K. Schoenning,[70] M. Scodeggio,[27a,27b] K. Y. Shan,[10,f] W. Shan,[22] X. Y. Shan,[66,53] J. F. Shangguan,[50] L. G. Shao,[1,58] M. Shao,[66,53] C. P. Shen,[10,f] H. F. Shen,[1,58] X. Y. Shen,[1,58] B. A. Shi,[58] H. C. Shi,[66,53] J. Y. Shi,[1] Q. Q. Shi,[50] R. S. Shi,[1,58] X. Shi,[1,53] X. D. Shi,[66,53] J. J. Song,[18] W. M. Song,[30,1] Y. X. Song,[42,g] S. Sosio,[69a,69c] S. Spataro,[69a,69c] F. Stieler,[31] K. X. Su,[71] P. P. Su,[50] Y. J. Su,[58] G. X. Sun,[1] H. Sun,[58] H. K. Sun,[1] J. F. Sun,[18] L. Sun,[71] S. S. Sun,[1,58] T. Sun,[1,58] W. Y. Sun,[30] X. Sun,[23,h] Y. J. Sun,[66,53] Y. Z. Sun,[1] Z. T. Sun,[45] Y. H. Tan,[71] Y. X. Tan,[66,53] C. J. Tang,[49] G. Y. Tang,[1] J. Tang,[54] L. Y. Tao,[67] Q. T. Tao,[23,h] M. Tat,[64] J. X. Teng,[66,53] V. Thoren,[70] W. H. Tian,[47] Y. Tian,[28,58] I. Uman,[57b] B. Wang,[1] B. L. Wang,[58] C. W. Wang,[38] D. Y. Wang,[42,g] F. Wang,[67] H. J. Wang,[34,j,k] H. P. Wang,[1,58] K. Wang,[1,53] L. L. Wang,[1] M. Wang,[45] M. Z. Wang,[42,g] Meng Wang,[1,58] S. Wang,[13] S. Wang,[10,f] T. Wang,[10,f] T. J. Wang,[39] W. Wang,[54] W. H. Wang,[71] W. P. Wang,[66,53] X. Wang,[42,g] X. F. Wang,[34,j,k] X. L. Wang,[10,f] Y. Wang,[56] Y. D. Wang,[41] Y. F. Wang,[1,53,58] Y. H. Wang,[43] Y. Q. Wang,[1] Yaqian Wang,[16,1] Z. Wang,[1,53] Z. Y. Wang,[1,58] Ziyi Wang,[58] D. H. Wei,[13] F. Weidner,[63] S. P. Wen,[1] D. J. White,[62] U. Wiedner,[4] G. Wilkinson,[64] M. Wolke,[70] L. Wollenberg,[4] J. F. Wu,[1,58] L. H. Wu,[1] L. J. Wu,[1,58] X. Wu,[10,f]

X. H. Wu,[30] Y. Wu,[66] Y. J. Wu,[28] Z. Wu,[1,53] L. Xia,[66,53] T. Xiang,[42,g] D. Xiao,[34,j,k] G. Y. Xiao,[38] H. Xiao,[10,f] S. Y. Xiao,[1] Y. L. Xiao,[10,f] Z. J. Xiao,[37] C. Xie,[38] X. H. Xie,[42,g] Y. Xie,[45] Y. G. Xie,[1,53] Y. H. Xie,[6] Z. P. Xie,[66,53] T. Y. Xing,[1,58] C. F. Xu,[1] C. J. Xu,[54] G. F. Xu,[1] H. Y. Xu,[61] Q. J. Xu,[15] X. P. Xu,[50] Y. C. Xu,[58] Z. P. Xu,[38] F. Yan,[10,f] L. Yan,[10,f] W. B. Yan,[66,53] W. C. Yan,[75] H. J. Yang,[46,e] H. L. Yang,[30] H. X. Yang,[1] L. Yang,[47] S. L. Yang,[58] Tao Yang,[1] Y. F. Yang,[39] Y. X. Yang,[1,58] Yifan Yang,[1,58] M. Ye,[1,53] M. H. Ye,[8] J. H. Yin,[1] Z. Y. You,[54] B. X. Yu,[1,53,58] C. X. Yu,[39] G. Yu,[1,58] T. Yu,[67] X. D. Yu,[42,g] C. Z. Yuan,[1,58] L. Yuan,[2] S. C. Yuan,[1] X. Q. Yuan,[1] Y. Yuan,[1,58] Z. Y. Yuan,[54] C. X. Yue,[35] A. A. Zafar,[68] F. R. Zeng,[45] X. Zeng,[6] Y. Zeng,[23,h] Y. H. Zhan,[54] A. Q. Zhang,[1] B. L. Zhang,[1] B. X. Zhang,[1] D. H. Zhang,[39] G. Y. Zhang,[18] H. Zhang,[66] H. H. Zhang,[54] H. H. Zhang,[30] H. Y. Zhang,[1,53] J. L. Zhang,[72] J. Q. Zhang,[37] J. W. Zhang,[1,53,58] J. X. Zhang,[34,j,k] J. Y. Zhang,[1] J. Z. Zhang,[1,58] Jianyu Zhang,[1,58] Jiawei Zhang,[1,58] L. M. Zhang,[56] L. Q. Zhang ,[54] Lei Zhang,[38] P. Zhang,[1] Q. Y. Zhang,[35,75] Shuihan Zhang,[1,58] Shulei Zhang,[23,h] X. D. Zhang,[41] X. M. Zhang,[1] X. Y. Zhang,[50] X. Y. Zhang,[45] Y. Zhang,[64] Y. T. Zhang,[75] Y. H. Zhang,[1,53] Yan Zhang,[66,53] Yao Zhang,[1] Z. H. Zhang,[1] Z. Y. Zhang,[71] Z. Y. Zhang,[39] G. Zhao,[1] J. Zhao,[35] J. Y. Zhao,[1,58] J. Z. Zhao,[1,53] Lei Zhao,[66,53] Ling Zhao,[1] M. G. Zhao,[39] Q. Zhao,[1] S. J. Zhao,[75] Y. B. Zhao,[1,53] Y. X. Zhao,[28,58] Z. G. Zhao,[66,53] A. Zhemchugov,[32,a] B. Zheng,[67] J. P. Zheng,[1,53] Y. H. Zheng,[58] B. Zhong,[37] C. Zhong,[67] X. Zhong,[54] H. Zhou,[45] L. P. Zhou,[1,58] X. Zhou,[71] X. K. Zhou,[58] X. R. Zhou,[66,53] X. Y. Zhou,[35] Y. Z. Zhou,[10,f] J. Zhu,[39] K. Zhu,[1] K. J. Zhu,[1,53,58] L. X. Zhu,[58] S. H. Zhu,[65] S. Q. Zhu,[38] T. J. Zhu,[72] W. J. Zhu,[10,f] Y. C. Zhu,[66,53] Z. A. Zhu,[1,58] B. S. Zou,[1] and J. H. Zou[1]

(BESIII Collaboration)

[1]*Institute of High Energy Physics, Beijing 100049, People's Republic of China*
[2]*Beihang University, Beijing 100191, People's Republic of China*
[3]*Beijing Institute of Petrochemical Technology, Beijing 102617, People's Republic of China*
[4]*Bochum Ruhr-University, D-44780 Bochum, Germany*
[5]*Carnegie Mellon University, Pittsburgh, Pennsylvania 15213, USA*
[6]*Central China Normal University, Wuhan 430079, People's Republic of China*
[7]*Central South University, Changsha 410083, People's Republic of China*
[8]*China Center of Advanced Science and Technology, Beijing 100190, People's Republic of China*
[9]*COMSATS University Islamabad, Lahore Campus,*
Defence Road, Off Raiwind Road, 54000 Lahore, Pakistan
[10]*Fudan University, Shanghai 200433, People's Republic of China*
[11]*G.I. Budker Institute of Nuclear Physics SB RAS (BINP), Novosibirsk 630090, Russia*
[12]*GSI Helmholtzcentre for Heavy Ion Research GmbH, D-64291 Darmstadt, Germany*
[13]*Guangxi Normal University, Guilin 541004, People's Republic of China*
[14]*Guangxi University, Nanning 530004, People's Republic of China*
[15]*Hangzhou Normal University, Hangzhou 310036, People's Republic of China*
[16]*Hebei University, Baoding 071002, People's Republic of China*
[17]*Helmholtz Institute Mainz, Staudinger Weg 18, D-55099 Mainz, Germany*
[18]*Henan Normal University, Xinxiang 453007, People's Republic of China*
[19]*Henan University of Science and Technology, Luoyang 471003, People's Republic of China*
[20]*Henan University of Technology, Zhengzhou 450001, People's Republic of China*
[21]*Huangshan College, Huangshan 245000, People's Republic of China*
[22]*Hunan Normal University, Changsha 410081, People's Republic of China*
[23]*Hunan University, Changsha 410082, People's Republic of China*
[24]*Indian Institute of Technology Madras, Chennai 600036, India*
[25]*Indiana University, Bloomington, Indiana 47405, USA*
[26a]*INFN Laboratori Nazionali di Frascati, I-00044, Frascati, Italy*
[26b]*INFN Sezione di Perugia, I-06100, Perugia, Italy*
[26c]*University of Perugia, I-06100, Perugia, Italy*
[27a]*INFN Sezione di Ferrara, I-44122, Ferrara, Italy*
[27b]*University of Ferrara, I-44122, Ferrara, Italy*
[28]*Institute of Modern Physics, Lanzhou 730000, People's Republic of China*
[29]*Institute of Physics and Technology, Peace Avenue 54B, Ulaanbaatar 13330, Mongolia*
[30]*Jilin University, Changchun 130012, People's Republic of China*
[31]*Johannes Gutenberg University of Mainz, Johann-Joachim-Becher-Weg 45, D-55099 Mainz, Germany*
[32]*Joint Institute for Nuclear Research, 141980 Dubna, Moscow region, Russia*
[33]*Justus-Liebig-Universitaet Giessen, II. Physikalisches Institut,*
Heinrich-Buff-Ring 16, D-35392 Giessen, Germany
[34]*Lanzhou University, Lanzhou 730000, People's Republic of China*

[35]Liaoning Normal University, Dalian 116029, People's Republic of China
[36]Liaoning University, Shenyang 110036, People's Republic of China
[37]Nanjing Normal University, Nanjing 210023, People's Republic of China
[38]Nanjing University, Nanjing 210093, People's Republic of China
[39]Nankai University, Tianjin 300071, People's Republic of China
[40]National Centre for Nuclear Research, Warsaw 02-093, Poland
[41]North China Electric Power University, Beijing 102206, People's Republic of China
[42]Peking University, Beijing 100871, People's Republic of China
[43]Qufu Normal University, Qufu 273165, People's Republic of China
[44]Shandong Normal University, Jinan 250014, People's Republic of China
[45]Shandong University, Jinan 250100, People's Republic of China
[46]Shanghai Jiao Tong University, Shanghai 200240, People's Republic of China
[47]Shanxi Normal University, Linfen 041004, People's Republic of China
[48]Shanxi University, Taiyuan 030006, People's Republic of China
[49]Sichuan University, Chengdu 610064, People's Republic of China
[50]Soochow University, Suzhou 215006, People's Republic of China
[51]South China Normal University, Guangzhou 510006, People's Republic of China
[52]Southeast University, Nanjing 211100, People's Republic of China
[53]State Key Laboratory of Particle Detection and Electronics,
Beijing 100049, Hefei 230026, People's Republic of China
[54]Sun Yat-Sen University, Guangzhou 510275, People's Republic of China
[55]Suranaree University of Technology, University Avenue 111, Nakhon Ratchasima 30000, Thailand
[56]Tsinghua University, Beijing 100084, People's Republic of China
[57a]Turkish Accelerator Center Particle Factory Group, Istinye University, 34010, Istanbul, Turkey
[57b]Near East University, Nicosia, North Cyprus, Mersin 10, Turkey
[58]University of Chinese Academy of Sciences, Beijing 100049, People's Republic of China
[59]University of Groningen, NL-9747 AA Groningen, The Netherlands
[60]University of Hawaii, Honolulu, Hawaii 96822, USA
[61]University of Jinan, Jinan 250022, People's Republic of China
[62]University of Manchester, Oxford Road, Manchester, M13 9PL, United Kingdom
[63]University of Muenster, Wilhelm-Klemm-Strasse 9, 48149 Muenster, Germany
[64]University of Oxford, Keble Road, Oxford OX13RH, United Kingdom
[65]University of Science and Technology Liaoning, Anshan 114051, People's Republic of China
[66]University of Science and Technology of China, Hefei 230026, People's Republic of China
[67]University of South China, Hengyang 421001, People's Republic of China
[68]University of the Punjab, Lahore-54590, Pakistan
[69a]University of Turin and INFN, University of Turin, I-10125, Turin, Italy
[69b]University of Eastern Piedmont, I-15121, Alessandria, Italy
[69c]INFN, I-10125, Turin, Italy
[70]Uppsala University, Box 516, SE-75120 Uppsala, Sweden
[71]Wuhan University, Wuhan 430072, People's Republic of China
[72]Xinyang Normal University, Xinyang 464000, People's Republic of China
[73]Yunnan University, Kunming 650500, People's Republic of China
[74]Zhejiang University, Hangzhou 310027, People's Republic of China
[75]Zhengzhou University, Zhengzhou 450001, People's Republic of China

[a]Also at the Moscow Institute of Physics and Technology, Moscow 141700, Russia.
[b]Also at the Novosibirsk State University, Novosibirsk, 630090, Russia.
[c]Also at the NRC "Kurchatov Institute", PNPI, 188300, Gatchina, Russia.
[d]Also at Goethe University Frankfurt, 60323 Frankfurt am Main, Germany.
[e]Also at Key Laboratory for Particle Physics, Astrophysics and Cosmology, Ministry of Education; Shanghai Key Laboratory for Particle Physics and Cosmology; Institute of Nuclear and Particle Physics, Shanghai 200240, People's Republic of China.
[f]Also at Key Laboratory of Nuclear Physics and Ion-beam Application (MOE) and Institute of Modern Physics, Fudan University, Shanghai 200443, People's Republic of China.
[g]Also at State Key Laboratory of Nuclear Physics and Technology, Peking University, Beijing 100871, People's Republic of China.
[h]Also at School of Physics and Electronics, Hunan University, Changsha 410082, China.
[i]Also at Guangdong Provincial Key Laboratory of Nuclear Science, Institute of Quantum Matter, South China Normal University, Guangzhou 510006, China.
[j]Also at Frontiers Science Center for Rare Isotopes, Lanzhou University, Lanzhou 730000, People's Republic of China.
[k]Also at Lanzhou Center for Theoretical Physics, Lanzhou University, Lanzhou 730000, People's Republic of China.
[l]Also at the Department of Mathematical Sciences, IBA, Karachi, Pakistan.

The singly Cabibbo suppressed decay $\Lambda_c^+ \to p\eta'$ is measured using 4.5 fb^{-1} of e^+e^- collision data collected at center-of-mass energies between 4.600 and 4.699 GeV with the BESIII detector at BEPCII. Evidence for $\Lambda_c^+ \to p\eta'$ with a statistical significance of 3.6σ is reported with a double-tag approach. The $\Lambda_c^+ \to p\eta'$ absolute branching fraction is determined to be $(5.62^{+2.46}_{-2.04} \pm 0.26) \times 10^{-4}$, where the first and second uncertainties are statistical and systematic, respectively. Our result is consistent with the branching fraction obtained by the Belle collaboration within the uncertainty of 1σ.

I. INTRODUCTION

The weak decays of the ground-state charmed baryon Λ_c^+ play an essential role in understanding the interplay of weak and strong interactions in the charm region [1]. In addition, information about the lightest charmed baryon provides key input for investigations of heavier charmed baryons [2] and bottom baryons [3,4]. In contrast to charmed meson decays, which are usually dominated by factorizable amplitudes, decays of charmed baryons receive sizable nonfactorizable contributions which arise from internal W emission and W exchange [5,6].

The complicated physics in charmed baryon decays is described by phenomenological model calculations, which strongly rely on experimental results. Experimentally, some Cabibbo favored decays [7–12] have been measured with relatively high precision, while the singly Cabibbo suppressed (SCS) decays are limited by statistics. Recently, measurements of SCS decay branching fractions have been carried out by the BESIII and Belle Collaborations [13–15]. The SCS decay $\Lambda_c^+ \to n\pi^+$ was observed for the first time at BESIII [16], and the measured branching fraction is consistent with the SU(3) prediction [17] but twice as large as that from current algebra [18].

The Belle Collaboration reported the first observation of the SCS decay $\Lambda_c^+ \to p\eta'$ with a statistical significance of 5.4σ and measured its decay branching fraction with respect to the $\Lambda_c^+ \to pK^-\pi^+$ to be $\mathcal{B}(\Lambda_c^+ \to p\eta')/\mathcal{B}(\Lambda_c^+ \to pK^-\pi^+) = (7.54 \pm 1.32 \pm 0.75) \times 10^{-3}$ [19]. The two-body SCS decay $\Lambda_c^+ \to p\eta'$ can proceed via the internal W-emission and W-exchange mechanisms, with the lowest-order Feynman diagrams shown in Fig. 1. The branching fraction of $\Lambda_c^+ \to p\eta'$ is predicted to be in the range of $10^{-3} - 10^{-4}$ [18]. To improve the knowledge of charmed baryons, more experimental studies of SCS decays are highly desirable.

In this paper we report a measurement of the absolute branching fraction of the SCS decay $\Lambda_c^+ \to p\eta'$ using 4.5 fb^{-1} of e^+e^- collision data collected with the BESIII detector at seven center-of-mass (CM) energies between 4.600 and 4.699 GeV. The $\Lambda_c^+\bar{\Lambda}_c^-$ datasets are above $\Lambda_c^+\bar{\Lambda}_c^-$ threshold and provide a clean environment with which to measure the absolute branching fractions of Λ_c^+. The CM energy and the integrated luminosity for each energy point are listed in Table I [20–22]. Throughout the text, the charge conjugate states are always implied.

II. BESIII DETECTOR AND MONTE CARLO SIMULATION

The BESIII detector [23] records symmetric e^+e^- collisions provided by the BEPCII storage ring [24] in the CM energy range from 2.0 to 4.95 GeV [25], with a peak luminosity of 1×10^{33} cm^{-2} s^{-1} achieved at CM energy of 3.77 GeV. BESIII has collected large data samples in this energy region [25]. The cylindrical core of the BESIII detector covers 93% of the full solid angle and consists of a multilayer drift chamber (MDC) operating with a helium-based gas mixture, a plastic scintillator time-of-flight system (TOF), and a CsI(Tl) electromagnetic calorimeter (EMC), which are all enclosed in a super-conducting solenoidal magnet providing a 1.0 T of magnetic field. The solenoid is supported by an octagonal flux-return yoke with resistive plate counter muon identification modules interleaved with steel. The charged-particle momentum resolution at 1 GeV/c is 0.5%, and the resolution of the ionization energy loss in the MDC (dE/dx) is 6% for electrons from Bhabha scattering. The EMC measures photon energies with a resolution of 2.5%
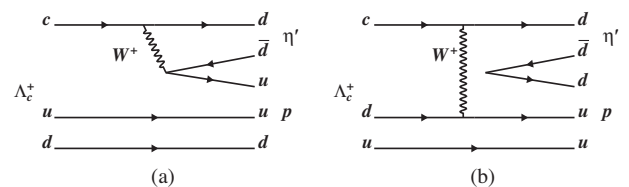
FIG. 1. Lowest-order Feynman diagrams for $\Lambda_c^+ \to p\eta'$ mediated via (a) W-emission and (b) W-exchange mechanisms.

TABLE I. The CM energy and the integrated luminosity ($\mathcal{L}_{\text{int}}$) for each energy point. The first and the second uncertainties are statistical and systematic, respectively.

Dataset	CM energy (MeV)	$\mathcal{L}_{\text{int}}$ (pb^{-1})
4600	$4599.53 \pm 0.07 \pm 0.74$	$586.90 \pm 0.10 \pm 3.90$
4612	$4611.86 \pm 0.12 \pm 0.32$	$103.83 \pm 0.05 \pm 0.55$
4628	$4628.00 \pm 0.06 \pm 0.32$	$521.52 \pm 0.11 \pm 2.76$
4641	$4640.91 \pm 0.06 \pm 0.38$	$552.41 \pm 0.12 \pm 2.93$
4661	$4661.24 \pm 0.06 \pm 0.29$	$529.63 \pm 0.12 \pm 2.81$
4682	$4681.92 \pm 0.08 \pm 0.29$	$1669.31 \pm 0.21 \pm 8.85$
4699	$4698.82 \pm 0.10 \pm 0.39$	$536.45 \pm 0.12 \pm 2.84$

(5%) at 1 GeV in the barrel (end-cap) region. The time resolution in the TOF barrel region is 68 ps. The end-cap TOF system was upgraded in 2015 using multigap resistive plate chamber technology, providing a time resolution of 60 ps [26].

Simulated data samples are produced with GEANT4-based [27] Monte Carlo (MC) software, which describes the geometry of the BESIII detector and simulates the performance of the detector. The signal MC samples of $e^+e^- \to \Lambda_c^+\bar{\Lambda}_c^-$ with $\bar{\Lambda}_c^-$ decaying into ten specific tag modes (as described below and listed in Table II) and $\Lambda_c^+ \to p\eta'$, which are used to determine the detection efficiencies, are generated for each individual CM energy using the generator KKMC [28] incorporating initial-state radiation (ISR) effects and the beam energy spread. The $\Lambda_c^+ \to p\eta'$ decay is modeled with a uniform phase-space distribution. The inclusive MC samples, which consist of $\Lambda_c^+\bar{\Lambda}_c^-$ events, charmed meson $D_{(s)}^{(*)}$ pair production, ISR return to the charmonium(-like) ψ states at lower masses, and continuum processes $e^+e^- \to q\bar{q}$ ($q = u, d, s$), are generated to estimate the potential background. Particle

decays are modeled with EVTGEN [29,30] using branching fractions taken from the Particle Data Group (PDG) [31], when available, or otherwise estimated with LUNDCHARM [32,33]. Final-state radiation from charged final-state particles is incorporated using PHOTOS [34].

III. METHODOLOGY

A double-tag (DT) approach [35] is implemented to study the SCS decay $\Lambda_c^+ \to p\eta'$. A data sample of $\bar{\Lambda}_c^-$ baryons, referred to as the single-tag (ST) sample, is reconstructed with ten exclusive hadronic decay modes, as listed in Table II. Events in which the signal decay $\Lambda_c^+ \to p\eta'$ is reconstructed in the system recoiling against the $\bar{\Lambda}_c^-$ candidates of the ST sample are denoted as DT candidates. The branching fraction of $\Lambda_c^+ \to p\eta'$ is determined as

$$\mathcal{B}(\Lambda_c^+ \to p\eta') = \frac{N_{\text{sig}}}{\mathcal{B}_{\text{inter}} \cdot \sum_{ij} N_{ij}^{\text{ST}} \cdot (\epsilon_{ij}^{\text{DT}}/\epsilon_{ij}^{\text{ST}})}, \quad (1)$$

where N_{sig} is the signal yield of the DT candidates and $\mathcal{B}_{\text{inter}}$ is the η' decay branching fraction taken from the PDG [31]. The subscripts i and j represent the ST modes and the data samples at different CM energies, respectively. The parameters N_{ij}^{ST}, $\epsilon_{ij}^{\text{ST}}$ and $\epsilon_{ij}^{\text{DT}}$ are the ST yields, ST and DT detection efficiencies, respectively.

IV. SINGLE-TAG EVENT SELECTIONS

The selection criteria of ST events are the same as Ref. [16]. Charged tracks detected in the MDC are required to be within a polar angle (θ) range of $|\cos\theta| < 0.93$, where θ is defined with respect to the z axis, which is the symmetry axis of the MDC. Except for tracks from K_S^0 and $\bar{\Lambda}$ decays, their distances of closest approach to the interaction point (IP) must be less than 10 cm along the z axis, and less than 1 cm in the transverse plane (referred to as a tight track hereafter). Particle identification (PID) is implemented by combining the measurements of dE/dx in the MDC and the flight time in the TOF, and each charged track is assigned a particle type of pion, kaon or proton, according to which assignment has the highest probability.

Photon candidates are identified from showers in the EMC. The deposited energy of each shower must be more than 25 MeV in the barrel region ($|\cos\theta| \leq 0.80$) or more than 50 MeV in the end-cap region ($0.86 \leq |\cos\theta| \leq 0.92$). To suppress electronic noise and showers unrelated to the event, the difference between the EMC time and the event start time is required to be within [0, 700] ns. A π^0 candidate is reconstructed with a photon pair within the invariant mass region (0.115, 0.150) GeV/c^2. To improve the resolution, a kinematic fit is performed by constraining the invariant mass of the photon pair to the world average

TABLE II. Branching fractions ($\mathcal{B}_{\text{ST}}$), ΔE requirement, ST yield, and ST detection efficiency of $\Lambda_c^+ \to p\eta'$ of each tag mode for the dataset 4682. The branching fractions have taken into account the intermediate particle decays, i.e., $\bar{\Lambda} \to \bar{p}\pi^+$, $\bar{\Sigma}^0 \to \gamma\bar{\Lambda}$, $\bar{\Sigma}^- \to \bar{p}\pi^0$, $K_S^0 \to \pi^+\pi^-$ and $\pi^0 \to \gamma\gamma$. The uncertainty in the ST yield is statistical only.

Tag mode	$\mathcal{B}_{\text{ST}}$ (%)	ΔE (MeV)	N_i^{ST}	ϵ_i^{ST} (%)
$\bar{p}K^+\pi^-$	6.28	$(-34, 20)$	$17,415 \pm 145$	47.3
$\bar{p}K_S^0$	1.10	$(-20, 20)$	$3,353 \pm 61$	48.1
$\bar{\Lambda}\pi^-$	0.83	$(-20, 20)$	$2,012 \pm 47$	37.8
$\bar{p}K^+\pi^-\pi^0$	4.41	$(-30, 20)$	$4,005 \pm 95$	14.5
$\bar{p}K_S^0\pi^0$	1.35	$(-30, 20)$	$1,454 \pm 52$	16.5
$\bar{\Lambda}\pi^-\pi^0$	4.48	$(-30, 20)$	$3,576 \pm 71$	14.6
$\bar{p}K_S^0\pi^+\pi^-$	1.11	$(-20, 20)$	$1,261 \pm 49$	17.7
$\bar{\Lambda}\pi^-\pi^+\pi^-$	2.33	$(-20, 20)$	$1,818 \pm 52$	12.3
$\bar{\Sigma}^0\pi^-$	0.82	$(-20, 20)$	$1,047 \pm 34$	19.3
$\bar{\Sigma}^-\pi^+\pi^-$	2.29	$(-30, 20)$	$2,275 \pm 63$	16.2

π^0 mass [31]. The momentum updated by the kinematic fit is used in further analysis.

Candidates for K_S^0 and $\bar{\Lambda}$ are reconstructed in their decays to $\pi^+\pi^-$ and $\bar{p}\pi^+$, respectively, where the charged tracks must have the distances of closest approach to the IP within 20 cm along the z axis (referred to as a loose track hereafter). To improve the signal purity, PID is required for the antiproton candidate, but not for the charged pion. The two daughter tracks are constrained to originate from a common decay vertex, and the χ^2 of the vertex fit is required to be less than 100. Furthermore, the decay vertex is required to be separated from the IP by a distance of at least twice the fitted vertex resolution. The momenta of the K_S^0 or $\bar{\Lambda}$ candidates updated by the fit are used in further analysis, and the invariant masses are required to be within $(0.487, 0.511)$ GeV/c^2 for $\pi^+\pi^-$ and $(1.111, 1.121)$ GeV/c^2 for $\bar{p}\pi^+$. The $\bar{\Sigma}^0$ and $\bar{\Sigma}^-$ candidates are reconstructed with the $\gamma\bar{\Lambda}$ and $\bar{p}\pi^0$ final states with invariant masses being within $(1.179, 1.203)$ and $(1.176, 1.200)$ GeV/c^2, respectively.

The ST $\bar{\Lambda}_c^-$ candidates are identified using the beam-constrained mass $M_{\mathrm{BC}} = \sqrt{E_{\mathrm{beam}}^2/c^4 - |\vec{p}_{\bar{\Lambda}_c^-}|^2/c^2}$ and energy difference $\Delta E = E_{\bar{\Lambda}_c^-} - E_{\mathrm{beam}}$, where E_{beam} is the beam energy and $E_{\bar{\Lambda}_c^-}$ and $\vec{p}_{\bar{\Lambda}_c^-}$ are the energy and momentum of the $\bar{\Lambda}_c^-$ candidate, respectively. The $\bar{\Lambda}_c^-$ candidates are required to satisfy tag-mode dependent asymmetric ΔE requirements, listed in Table II, which take into account the effects of ISR and correspond to three times the resolution around the peak. If there is more than one candidate satisfying the above requirements for a specific tag mode, the one with the minimum $|\Delta E|$ is kept, and those with $M_{\mathrm{BC}} \in (2.275, 2.310)$ GeV/c^2 are retained for further analysis.

For the $\bar{\Lambda}_c^- \to \bar{p}K_S^0\pi^0$ ST mode, candidate events with $M_{\bar{p}\pi^+} \in (1.100, 1.125)$ GeV/c^2 and $M_{\bar{p}\pi^0} \in (1.170, 1.200)$ GeV/c^2 are vetoed to avoid double counting with the $\bar{\Lambda}_c^- \to \bar{\Lambda}\pi^-\pi^0$ or $\bar{\Lambda}_c^- \to \bar{\Sigma}^-\pi^+\pi^-$ ST modes, respectively. For the $\bar{\Lambda}_c^- \to \bar{\Sigma}^-\pi^+\pi^-$ ST mode, candidate events with $M_{\pi^+\pi^-} \in (0.490, 0.510)$ GeV/c^2 and $M_{\bar{p}\pi^+} \in (1.110, 1.120)$ GeV/c^2 are rejected to avoid double counting with the $\bar{\Lambda}_c^- \to \bar{p}K_S^0\pi^0$ or $\bar{\Lambda}_c^- \to \bar{\Lambda}\pi^-\pi^0$ ST modes, respectively. In the $\bar{\Lambda}_c^- \to \bar{p}K_S^0\pi^+\pi^-$ and $\bar{\Lambda}\pi^-\pi^+\pi^-$ selections, candidate events with $M_{\bar{p}\pi^+} \in (1.100, 1.125)$ GeV/c^2 and $M_{\pi^+\pi^-} \in (0.490, 0.510)$ GeV/c^2 are rejected, respectively.

The M_{BC} distributions of candidates for the ten ST modes with the dataset 4682 are illustrated in Fig. 2, where clear $\bar{\Lambda}_c^-$ signals are observed in each ST mode. No peaking background is found with the investigation of the inclusive MC samples. To obtain the ST yields, unbinned maximum likelihood fits on these M_{BC} distributions are performed, where the signal shape is modeled with the MC-simulated shape convolved with a Gaussian function representing
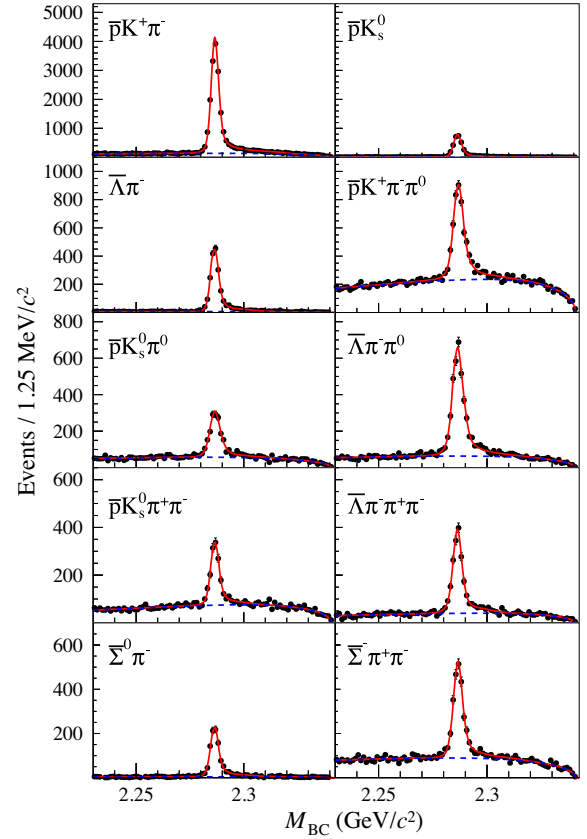

FIG. 2. The M_{BC} distributions of the ST modes for the dataset 4680. The points with error bars represent data. The (red) solid curves indicate the fit results and the (blue) dashed curves describe the background shapes.

the resolution difference between data and MC simulation. The parameters of the Gaussian function are determined in the fit, and the resultant standard deviations are varied between 0.1 and 0.7 MeV/c^2 for different ST modes. The background shape is described by an ARGUS function [36], fixing the end-point parameter to the corresponding E_{beam}. The signal yields for the individual ST modes are summarized in Table II. The same procedure is performed for the other six data samples at different CM energies, and the results can be found in Ref. [16] and its supplemental material. The sum of ST yields for all data samples at different CM energies is $(1.0524 \pm 0.0038) \times 10^5$, where the uncertainty is statistical.

V. SIGNAL RECONSTRUCTION

Candidates for the signal decay $\Lambda_c^+ \to p\eta'$ are selected with the remaining tracks recoiling against the $\bar{\Lambda}_c^-$ candidates. The η' meson is reconstructed in its two most prominent decay modes, $\eta' \to \pi^+\pi^-\eta$ and $\pi^+\pi^-\gamma$, where the η meson is reconstructed with its neutral decay modes, *i.e.* $\eta \to 2\gamma$ and $\eta \to 3\pi^0$, corresponding to (72.12 ± 0.34) % [31] of η decays.
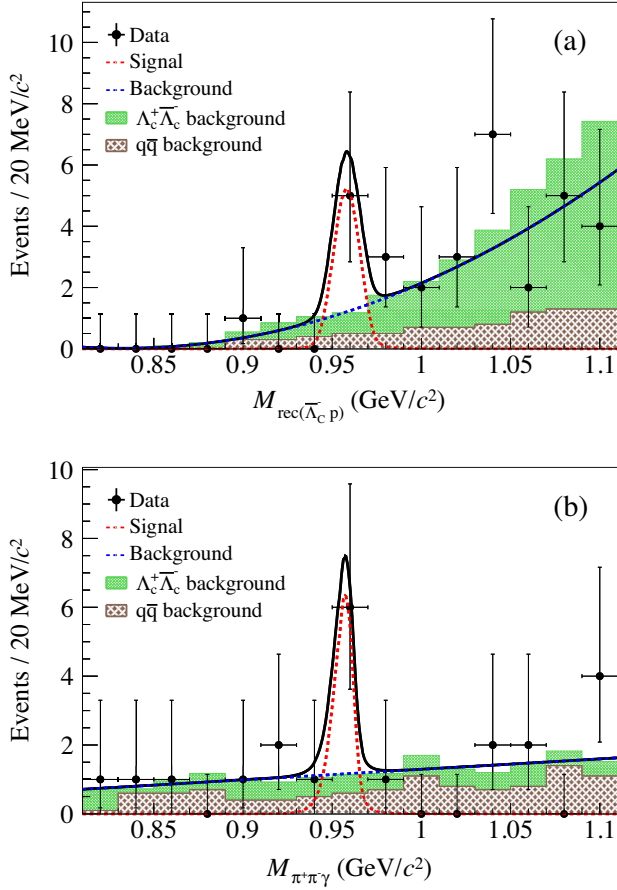
FIG. 3. Simultaneous fit to (a) the $M_{\text{rec}(\bar{\Lambda}_c^- p)}$ distribution in the $\eta' \to \pi^+ \pi^- \eta$ mode and (b) the $M_{\pi^+ \pi^- \gamma}$ distribution in the $\eta' \to \pi^+ \pi^- \gamma$ mode with the combined seven data samples. The black points with error bars are data. The red and blue dashed lines indicate the curves for the signal and background, respectively. The black line is the sum over all the components in the fit. The brown and green hatched histograms for the two background components are from the inclusive MC samples.

For both η' decay modes, the signal side is required to include exactly three tight tracks, which are then identified with PID to be p, π^+, π^-. To suppress contamination from long-lifetime particles in the final state, the candidate events are further required to not contain any loose tracks. Possible background from $\Lambda \to p\pi^-$ is rejected completely by requiring $M_{p\pi^-} > 1.125$ GeV/c^2, and candidate events with $M_{\pi^+\pi^-} \in (0.490, 0.510)$ GeV/c^2 are vetoed to reduce the $K_S^0 \to \pi^+\pi^-$ background by 86%.

For the reconstruction mode of $\eta' \to \pi^+ \pi^- \eta$, to increase the detection efficiency, the neutral decays of η are not reconstructed with individual final states, but considered as missing. Thus, the η signal is selected in the system recoiling against the ST $\bar{\Lambda}_c^-$, p, π^+ and π^-. To improve the mass resolution, we use $M_{\text{rec}(\bar{\Lambda}_c^- p\pi^+\pi^-)} + M_{\bar{\Lambda}_c^-} - m_{\Lambda_c^+}$ instead of $M_{\text{rec}(\bar{\Lambda}_c^- p\pi^+\pi^-)}$ to reconstruct the η signal, where $M_{\text{rec}(\bar{\Lambda}_c^- p\pi^+\pi^-)}$ is the recoiling mass against the ST $\bar{\Lambda}_c^-$, p, π^+

and π^-, $M_{\bar{\Lambda}_c^-}$ is the reconstructed mass of the $\bar{\Lambda}_c^-$ candidate, and $m_{\Lambda_c^+}$ is the world average Λ_c^+ mass [31]. The $M_{\text{rec}(\bar{\Lambda}_c^- p\pi^+\pi^-)}$ variable is required to be within the η mass interval $(0.533, 0.561)$ GeV/c^2, corresponding to 1σ resolution of the recoiling mass, to reject the $\Lambda_c^+ \to pK_L^0\pi^+\pi^-$ background. The recoiling mass against the ST $\bar{\Lambda}_c^-$ is required to be within $(2.275, 2.310)$ GeV/c^2. Finally, the signal yield of $\Lambda_c^+ \to p\eta'$ is determined by fitting the distribution of $M_{\text{rec}(\bar{\Lambda}_c^- p)}$, which is defined as the recoiling mass against the ST $\bar{\Lambda}_c^-$ and p, as presented in Fig. 3(a).

For the reconstruction mode of $\eta' \to \pi^+ \pi^- \gamma$, the γ candidates are selected from photons not assigned to ST π^0s, and the one with the minimum value of $|\Delta E_{p\pi^+\pi^-\gamma}|$ is kept for further analysis, where $\Delta E_{p\pi^+\pi^-\gamma} = E_{p\pi^+\pi^-\gamma} - E_{\text{beam}}$ and $E_{p\pi^+\pi^-\gamma}$ is the reconstructed energy of the candidate events. The candidate events are further required to be within $\Delta E_{p\pi^+\pi^-\gamma} \in (-0.017, 0.008)$ GeV. The background containing extra π^0s is vetoed with the requirement of $M_{\text{rec}(\bar{\Lambda}_c^- p\pi^+\pi^-)} < 0.1$ GeV/c^2. Additionally, the γ is selected with $\alpha_\gamma < 20°$, where α_γ is the angle between γ and the direction of recoiling system of ST $\bar{\Lambda}_c^-$, p, π^+ and π^-. Furthermore, the invariant mass of $p\pi^+\pi^-\gamma$ is required to be within $M_{p\pi^+\pi^-\gamma} \in (2.275, 2.310)$ GeV/c^2. Finally, the signal yield of $\Lambda_c^+ \to p\eta'$ is determined by fitting the distribution of $M_{\pi^+\pi^-\gamma}$, as presented in Fig. 3(b).

VI. BACKGROUND ANALYSIS

The potential background events are classified into two categories: those directly originating from continuum hadron production in the e^+e^- annihilation (denoted as $q\bar{q}$ background hereafter) and those from the $e^+e^- \to \Lambda_c^+\bar{\Lambda}_c^-$ events (denoted as $\Lambda_c^+\bar{\Lambda}_c^-$ background hereafter). The distributions and magnitudes of $q\bar{q}$ and $\Lambda_c^+\bar{\Lambda}_c^-$ backgrounds are estimated with the inclusive MC samples. The main residual background sources are $\Lambda_c^+ \to pK_L^0\pi^+\pi^-$, $\Lambda_c^+ \to \Sigma^+\eta$ and $\Lambda_c^+ \to \Sigma^+\omega$. The resultant $M_{\text{rec}(\bar{\Lambda}_c^- p)}$ and $M_{\pi^+\pi^-\gamma}$ distributions of the accepted candidates in data are depicted in Fig. 3. There are small peaks in the η' signal regions for both decay modes. The simulated shapes, which display no peaking background, describe the backgrounds well.

VII. BRANCHING FRACTION MEASUREMENT

The branching fraction of $\Lambda_c^+ \to p\eta'$ is determined with Eq. (1) by performing a simultaneous unbinned maximum likelihood fit on the distributions of $M_{\text{rec}(\bar{\Lambda}_c^- p)}$ and $M_{\pi^+\pi^-\gamma}$ in the two η' decay modes, constrained to the same $\mathcal{B}(\Lambda_c^+ \to p\eta')$ and taking into account different detection efficiencies and branching fractions of η'. The signal shapes are modeled by the MC-simulated shapes. The background shapes are described by second-order polynomial functions with fixed parameters, which are obtained by fitting the

TABLE III.   The DT detection efficiencies in percentage in the $\eta' \to \pi^+\pi^-\eta$ mode for the ten tag modes and seven datasets at different CM energies. The statistical uncertainties are lower than 0.3%.

Dataset	4600	4612	4628	4641	4661	4682	4699
$\bar{p}K^+\pi^-$	16.1	14.8	14.1	14.2	13.5	13.2	12.9
$\bar{p}K^0_S$	18.6	15.6	15.7	14.8	14.5	14.1	14.3
$\bar{\Lambda}\pi^-$	15.2	12.8	12.3	11.7	11.7	10.9	10.4
$\bar{p}K^+\pi^-\pi^0$	3.9	3.7	3.4	3.3	3.3	3.2	3.2
$\bar{p}K^0_S\pi^0$	5.3	4.5	4.6	4.2	4.5	3.8	4.0
$\bar{\Lambda}\pi^-\pi^0$	4.7	3.8	3.6	3.6	3.4	3.2	3.2
$\bar{p}K^0_S\pi^+\pi^-$	6.3	5.3	5.1	4.9	4.5	4.8	4.6
$\bar{\Lambda}\pi^-\pi^+\pi^-$	3.8	3.2	3.4	3.1	2.9	3.2	2.8
$\bar{\Sigma}^0\pi^-$	6.3	5.8	5.7	5.0	4.4	4.2	4.5
$\bar{\Sigma}^-\pi^+\pi^-$	5.3	4.7	4.7	4.3	4.1	3.9	4.0

corresponding distributions of inclusive MC samples, and the background yields are floating. The fit curves are depicted in Fig. 3. In Eq. (1), the $\mathcal{B}_{\mathrm{inter}}$ values are $(30.7 \pm 0.4)\%$ and $(29.5 \pm 0.4)\%$ for the modes of $\eta' \to \pi^+\pi^-\eta$ and $\eta' \to \pi^+\pi^-\gamma$, respectively, the ST detection efficiency $\epsilon^{\mathrm{ST}}_{ij}$ is obtained with the same procedure as in Ref. [16], and the DT detection efficiency $\epsilon^{\mathrm{DT}}_{ij}$ is derived with the signal MC samples. The efficiencies are summarized in Tables III and IV for the $\eta' \to \pi^+\pi^-\eta$ and $\pi^+\pi^-\gamma$ decay modes, respectively. The statistical significance of $\Lambda^+_c \to p\eta'$ is 3.6σ, which is calculated from the change of the likelihood values between the fits with and without the signal component included, and accounting for the change in the number of degrees of freedom. The branching fraction of $\Lambda^+_c \to p\eta'$ is determined to be $\mathcal{B}(\Lambda^+_c \to p\eta') = (5.62^{+2.46}_{-2.04}) \times 10^{-4}$, corresponding to signal yields of $4.9^{+3.2}_{-2.6}$ and $4.3^{+2.6}_{-2.2}$ for the $\eta' \to \pi^+\pi^-\eta$ and $\pi^+\pi^-\gamma$ modes, where the uncertainties are statistical.

TABLE IV.   The DT detection efficiencies in percentage in the $\eta' \to \pi^+\pi^-\gamma$ mode for ten tag modes and seven datasets at different CM energies. The statistical uncertainties are lower than 0.3%.

Dataset	4600	4612	4628	4641	4661	4682	4699
$\bar{p}K^+\pi^-$	13.7	13.0	12.4	12.4	12.1	11.7	11.5
$\bar{p}K^0_S$	15.4	14.3	14.0	14.6	13.4	12.7	12.5
$\bar{\Lambda}\pi^-$	13.2	11.0	10.4	10.6	10.8	9.9	9.8
$\bar{p}K^+\pi^-\pi^0$	3.7	3.5	3.4	3.3	3.3	3.2	3.2
$\bar{p}K^0_S\pi^0$	4.2	4.3	4.5	4.3	3.8	4.1	4.0
$\bar{\Lambda}\pi^-\pi^0$	4.1	3.8	3.6	3.4	3.4	3.1	3.2
$\bar{p}K^0_S\pi^+\pi^-$	5.4	4.8	4.4	4.6	4.8	4.8	4.6
$\bar{\Lambda}\pi^-\pi^+\pi^-$	3.7	3.4	3.1	3.0	3.0	3.0	3.0
$\bar{\Sigma}^0\pi^-$	6.9	5.0	5.4	5.0	4.5	5.1	4.5
$\bar{\Sigma}^-\pi^+\pi^-$	4.6	4.4	4.3	3.8	3.8	3.8	3.9

VIII. SYSTEMATIC UNCERTAINTY

The systematic uncertainties for the branching fraction measurement comprise those associated with the ST yields (N^{ST}_{ij}), detection efficiencies of the ST $\bar{\Lambda}^-_c$ $(\epsilon^{\mathrm{ST}}_{ij})$, detection efficiencies of the DT events $(\epsilon^{\mathrm{DT}}_{ij})$ and signal yield (N_{sig}). As the DT technique is adopted, the systematic uncertainties originating from reconstructing the ST side largely cancel. The systematic uncertainties are evaluated relative to the measured branching fraction. The details are described in the following.

The uncertainties associated with the tracking and PID efficiencies for the proton and π are determined with the control samples $J/\psi \to p\bar{p}\pi^+\pi^-$ [37] and $J/\psi \to \pi^+\pi^-\pi^0$ [38], respectively. The systematic uncertainties for tracking and PID are both assigned to be 1.0% for each proton and π, respectively.

The uncertainty in the reconstruction efficiency for the γ in the $\eta' \to \pi^+\pi^-\gamma$ decay mode is assigned to be 1.0% based on a study with the control sample $J/\psi \to \rho^0\pi^0$ events [39].

The uncertainty in the ST yields is 0.5%, which arises from the statistical uncertainty and the fits to the M_{BC} distributions. The uncertainty in the fitting procedure is evaluated by floating the truncation parameter of the ARGUS function and changing the single Gaussian function to a double Gaussian function.

The systematic uncertainty of the $M_{\mathrm{rec}(\bar{\Lambda}^-_c p\pi^+\pi^-)}$ requirement for the $\eta' \to \pi^+\pi^-\eta$ decay mode is estimated by correcting the variable $M_{\mathrm{rec}(\bar{\Lambda}^-_c p\pi^+\pi^-)}$ in the MC samples according to the observed resolution difference between data and MC simulation. The resolution difference is studied with the control sample $\Lambda^+_c \to pK^0_L\pi^+\pi^-$. The change of the obtained efficiency of the corrected MC samples from the nominal efficiency, 1.3%, is taken as the corresponding systematic uncertainty.

The systematic uncertainty due to the $\Delta E_{p\pi^+\pi^-\gamma}$ requirement for the $\eta' \to \pi^+\pi^-\gamma$ decay mode is studied with the control sample $\Lambda^+_c \to \Sigma^0\pi^+$ with $\Sigma^0 \to \Lambda\gamma$, which has a similar final state as the signal process. The difference between the efficiency in MC simulation and that in the control sample, 1.1%, is assigned to be the systematic uncertainty.

The systematic uncertainties arising from the $M_{\mathrm{rec}(\bar{\Lambda}^-_c p\pi^+\pi^-)}$ and α_γ requirements for the $\eta' \to \pi^+\pi^-\gamma$ decay mode are studied with the control sample $\Lambda^+_c \to pK^0_S\pi^0$. The differences of the efficiencies between data and MC simulation, 1.3 and 0.8%, are taken as the systematic uncertainties due to the $M_{\mathrm{rec}(\bar{\Lambda}^-_c p\pi^+\pi^-)}$ and α_γ requirements, respectively.

The uncertainty in the fit strategy of $M_{\mathrm{rec}(\bar{\Lambda}^-_c p)}$ and $M_{\pi^+\pi^-\gamma}$ is assigned to be 2.9%, which is estimated by shifting the fit range higher by 50 MeV and varying the background shape to a third-order polynomial function.

TABLE V. The relative systematic uncertainties in percent for $\Lambda_c^+ \to p\eta'$ in the decay modes of $\eta' \to \pi^+\pi^-\eta$ and $\eta' \to \pi^+\pi^-\gamma$.

Source	$\pi^+\pi^-\eta$	$\pi^+\pi^-\gamma$
p tracking		1.0
p PID		1.0
π tracking		2.0
π PID		2.0
ST yield		0.5
$M_{\mathrm{rec}(\bar{\Lambda}_c^- p\pi^+\pi^-)}$ requirement		1.3
Fit strategy		2.9
Tag bias		0.9
γ detection	$\cdots$	1.0
$\Delta E_{p\pi^+\pi^-\gamma}$ requirement	$\cdots$	1.1
α_γ requirement	$\cdots$	0.8
$\mathcal{B}_{\mathrm{inter}}$	0.5	0.4
Signal shape	0.6	0.1
Signal modeling	0.1	1.0
Total	4.7	5.0

TABLE VI. Comparison of the measured branching fraction (in 10^{-4}) of $\Lambda_c^+ \to p\eta'$ to theoretical predictions and the Belle result.

	$\Lambda_c^+ \to p\eta'$
BESIII	$5.62^{+2.46}_{-2.04} \pm 0.26$
Belle [19]	4.73 ± 0.97
Sharma *et al.* [41]	4–6
Uppal *et al.* [42]	0.4–2
Geng *et al.* [17]	$12.2^{+14.3}_{-8.7}$

IX. SUMMARY

In summary, the SCS decay $\Lambda_c^+ \to p\eta'$ is observed with a statistical significance of 3.6σ by using e^+e^- collision data samples corresponding to a total integrated luminosity of $4.5~\mathrm{fb}^{-1}$ collected at seven CM energies between 4.600 and 4.699 GeV with the BESIII detector. The absolute branching fraction of $\Lambda_c^+ \to p\eta'$ is measured to be $(5.62^{+2.46}_{-2.04} \pm 0.26) \times 10^{-4}$, where the first and second uncertainties are statistical and systematic, respectively. The branching fraction measured in this work is consistent with the Belle result [19] and the predictions in Refs. [17,41], but significantly higher than that in Ref. [42], as shown in Table VI. The result from this analysis provides an input to understand the dynamics of charmed baryon decays, and helps to improve different theoretical models.

The systematic uncertainties due to the signal shape for the $\eta' \to \pi^+\pi^-\eta$ and $\eta' \to \pi^+\pi^-\gamma$ decay modes are studied with the control samples $\Lambda_c^+ \to pK_S^0$ and $\Lambda_c^+ \to \Sigma^0\pi^+$ with $\Sigma^0 \to \Lambda\gamma$, respectively. The distributions of $M_{\mathrm{rec}(\bar{\Lambda}_c^- p)}$ and M_{Σ^0} are fitted by MC shapes, with or without a convolution with a Gaussian function. The differences of yields between the two cases, 0.6 and 0.1%, are taken as the corresponding systematic uncertainties for the two modes, respectively.

The systematic uncertainty arising from the signal modeling is investigated by generating a new set of signal MC $\Lambda_c^+ \to p\eta'$ events, with proton polar-angle distribution parametrized by $1 + \alpha\cos^2\theta$ [40] with decay parameter $\alpha = \pm 1$. Here θ is the polar angle of the proton with respect to the Λ_c^+ in the e^+e^- CM system. Comparing the differences in detection efficiencies between the nominal and alternative samples, the resultant uncertainties are obtained to be 1.0% for the $\eta' \to \pi^+\pi^-\gamma$ decay mode, and 0.1% for the $\eta' \to \pi^+\pi^-\eta$ mode.

The uncertainties in the branching fractions of the intermediate state decays from the PDG [31] are 0.5 and 0.4% for the $\eta' \to \pi^+\pi^-\eta$ and $\eta' \to \pi^+\pi^-\gamma$ decay modes, respectively.

According to Eq. (1), the uncertainty related to the ST efficiency mostly cancels. However, due to different multiplicities, the ST efficiencies estimated with the generic and signal MC samples are expected to differ from each other slightly and result in a so-called "tag bias" uncertainty. The difference between the ST efficiencies given by the generic and signal MC samples, 0.9%, is assigned as the corresponding uncertainty.

Table V summarizes the individual relative systematic uncertainties, where the correlated systematic uncertainties are listed in the top and the uncorrelated systematic uncertainties are listed in the bottom.

[1] H. Y. Cheng, Front. Phys. **10**, 101406 (2015).
[2] F. S. Yu, H.-Y. Jiang, R.-H. Li, C.-D. Lü, W. Wang, and Z.-X. Zhao, Chin. Phys. C **42**, 051001 (2018).
[3] R. Dutta, Phys. Rev. D **93**, 054003 (2016).
[4] W. Detmold, C. Lehner, and S. Meinel, Phys. Rev. D **92**, 034503 (2015).
[5] L. L. Chau and H. Y. Cheng, Phys. Rev. Lett. **56**, 1655 (1986).
[6] Y. Kohara, Phys. Rev. D **44**, 2799 (1991).
[7] A. Zupanc *et al.*, Phys. Rev. Lett. **113**, 042002 (2014).
[8] M. Ablikim *et al.* (BESIII Collaboration), Phys. Rev. Lett. **116**, 052001 (2016).
[9] M. Ablikim *et al.* (BESIII Collaboration), Phys. Rev. Lett. **118**, 112001 (2017).
[10] B. Pal *et al.* (Belle Collaboration), Phys. Rev. D **96**, 051102 (2017).
[11] M. Ablikim *et al.* (BESIII Collaboration), Chin. Phys. C **43**, 083002 (2019).
[12] M. Ablikim *et al.* (BESIII Collaboration), Phys. Lett. B **817**, 136327 (2021).
[13] M. Ablikim *et al.* (BESIII Collaboration), Phys. Rev. Lett. **117**, 232002 (2016).
[14] M. Ablikim *et al.* (BESIII Collaboration), Phys. Rev. D **95**, 111102 (2017).
[15] S. X. Li *et al.* (Belle Collaboration), Phys. Rev. D **103**, 072004 (2021).
[16] M. Ablikim *et al.* (BESIII Collaboration), Phys. Rev. Lett. **128**, 142001 (2022).
[17] C. Q. Geng, C.-W. Liu, and T.-H. Tsai, Phys. Lett. B **790**, 225 (2019).
[18] H. Y. Cheng, X.-W. Kang, and F. Xu, Phys. Rev. D **97**, 074028 (2018).
[19] S. X. Li *et al.* (Belle Collaboration), J. High Energy Phys. 03 (2022) 090.
[20] M. Ablikim *et al.* (BESIII Collaboration), Chin. Phys. C **40**, 063001 (2016).
[21] M. Ablikim *et al.* (BESIII Collaboration), arXiv:2203.03133.
[22] M. Ablikim *et al.* (BESIII Collaboration), arXiv:2205.04809.
[23] M. Ablikim *et al.* (BESIII Collaboration), Nucl. Instrum. Methods Phys. Res., Sect. A **614**, 345 (2010).
[24] C. H. Yu *et al.*, *Proceedings of the IPAC2016, Busan, Korea* (JACoW, Geneva, Switzerland, 2016), https://accelconf.web.cern.ch/ipac2016/doi/JACoW-IPAC2016-TUYA01.html.
[25] M. Ablikim *et al.* (BESIII Collaboration), Chin. Phys. C **44**, 040001 (2020).
[26] X. Li *et al.*, Radiat. Detect. Technol. Methods **1**, 13 (2017); Y. X. Guo *et al.*, Radiat. Detect. Technol. Methods **1**, 15 (2017).
[27] S. Agostinelli *et al.*, Nucl. Instrum. Methods Phys. Res., Sect. A **506**, 250 (2003).
[28] S. Jadach, B. F. L. Ward, and Z. Wąs, Phys. Rev. D **63**, 113009 (2001).
[29] D. J. Lange, Nucl. Instrum. Methods Phys. Res., Sect. A **462**, 152 (2001).
[30] R. G. Ping, Chin. Phys. C **32**, 599 (2008).
[31] P. A. Zyla *et al.* (Particle Data Group), Prog. Theor. Exp. Phys. **2020**, 083C01 (2020) and 2021 update.
[32] J. C. Chen, G. S. Huang, X. R. Qi, D. H. Zhang, and Y. S. Zhu, Phys. Rev. D **62**, 034003 (2000).
[33] R. L. Yang, R. G. Ping, and H. Chen, Chin. Phys. Lett. **31**, 061301 (2014).
[34] B. Richter-Was, Phys. Lett. B **303**, 163 (1993).
[35] J. Adler *et al.*, Phys. Rev. Lett. **62**, 1821 (1989).
[36] H. Albrecht *et al.* (ARGUS Collaboration), Phys. Lett. B **241**, 278 (1990).
[37] M. Ablikim, X.-C. Ai, X.-B. Ji, S.-J. Chen, Y. Zhang, L.-H. Wu, L.-L. Wang, and Y. Yuan (BESIII Collaboration), Chin. Phys. C **40**, 026201 (2016).
[38] M. Ablikim *et al.* (BESIII Collaboration), Phys. Rev. D **96**, 112012 (2017).
[39] M. Ablikim *et al.* (BESIII Collaboration), Phys. Rev. D **83**, 012003 (2011).
[40] M. Ablikim *et al.* (BESIII Collaboration), Phys. Rev. D **100**, 072004 (2019).
[41] K. K. Sharma, and R. C. Verma, Phys. Rev. D **55**, 7067 (1997).
[42] T. Uppal, R. C. Verna, and M. P. Khanna, Phys. Rev. D **49**, 3417 (1994).